molbank

IMPACT FACTOR 0.4

CITESCORE 0.9

Communication

Molecular Structure of the Monohydrate Hydrochloride Salt of the Antimalarial Drug Chloroquine

Silvia Rizzato and Massimo Moret

MDPI

https://doi.org/10.3390/M2131

molbank

MDPI

Communication

Molecular Structure of the Monohydrate Hydrochloride Salt of the Antimalarial Drug Chloroquine

Silvia Rizzato [1,*] and Massimo Moret [2]

[1] Dipartimento di Chimica, Università Degli Studi di Milano, Via C. Golgi 19, 20133 Milano, Italy
[2] Dipartimento di Scienza dei Materiali, Università Degli Studi di Milano-Bicocca, Via R. Cozzi 55, 20125 Milano, Italy; massimo.moret@unimib.it
* Correspondence: silvia.rizzato@unimi.it; Tel.: +39-02-50314464

Abstract

We report the crystallization and single-crystal X-ray analysis of the monohydrate hydrochloride salt of chloroquine(CQ), abbreviated **CQHCl·H_2O**, an antimalarial drug with the formula $C_{18}H_{26}ClN_3$. The crystal structure reveals a well-defined supramolecular architecture stabilized by an extensive hydrogen-bonding network involving CQH^+ cations, chloride anions, and water molecules. Notably, this study provides the first crystallographic characterization of a monoprotonated chloroquine salt. Additionally, our findings demonstrate the feasibility of isolating pseudo-polymorphic forms of a commercially available CQ salt via heterogeneous crystallization.

Keywords: crystal structure; hydrogen bond; chloroquine; antimalarial; heterogeneous crystallization

1. Introduction

Chloroquine (CQ) is a well-established antimalarial agent that is also widely used in the treatment of autoimmune diseases, including rheumatoid arthritis [1]. Along with its derivative hydroxychloroquine (HCQ), CQ has been extensively studied for potential antiviral activity, with efficacy demonstrated in both cell-culture systems and animal models. Owing to these properties, CQ and HCQ were among the earliest compounds investigated as experimental therapeutic candidates during the initial stages of the COVID-19 pandemic [2,3]; however, subsequent studies did not confirm their clinical efficacy, and their use is no longer recommended.

Chloroquine is an amphiphilic weak base that exists in both charged and uncharged forms. The molecule can adopt the following three protonation states: the neutral species (CQ^0), the monoprotonated species (CQH^+), and the diprotonated species (CQH_2^{2+}). The two basic ionization sites have pK_a values of 8.4 and 10.8 at 20 °C, corresponding to the aromatic nitrogen and the tertiary diethylamino nitrogen, respectively [4]. Under acidic or neutral conditions, chloroquine is largely protonated; however, at physiological pH (7.4), approximately 18% of the molecules are already in the monoprotonated form [5]. In its deprotonated state, chloroquine can undergo prototropic tautomerism between amino and imino forms [6].

Pharmaceutical compounds such as CQ could exist in different chemical and solid-state forms that can significantly influence the bioavailability and the overall stability of the drug product as well as impact its manufacturability and storage properties [7]. One common approach is the formulation of an active ingredient such as salt which can

Academic Editor: R. Alan Aitken

Received: 29 December 2025
Revised: 23 January 2026
Accepted: 30 January 2026
Published: 3 February 2026

be produced using a variety of counterions, although their choice is limited by toxicity criteria. For molecules with multiple protonation sites, salts corresponding to different protonation states can be obtained; for each one, different distinct hydration levels are potentially possible.

Chloroquine is typically administered as diphosphate or phosphate salt and all commercially available formulations contain the racemic mixture [8]. Bioactivity data have also been reported for the sulphate, disulphate, and hydrochloride salts; these products are usually for in vitro studies and are not formulated for therapeutic use, although the hydrochloride form has been used for intramuscular injection in cases of malaria-induced coma [9]. Structural characterization has been carried out exclusively for the diphosphate salt at different degrees of hydration, in which chloroquine is present in the dicationic state [10–12]. To date, no specific information is available regarding the protonation state of chloroquine in other available salt forms.

The title compound **CQHCl·H$_2$O** (N^4-(7-chloroquinolin-4-yl)-N^1,N^1-diethylpentane-1,4-diaminehydrochloride monohydrate) (Scheme 1) constitutes the first crystallographically characterized salt with chloride as the counterion and above all featuring monoprotonated chloroquine. Accordingly, its solid-state characterization is of considerable significance.

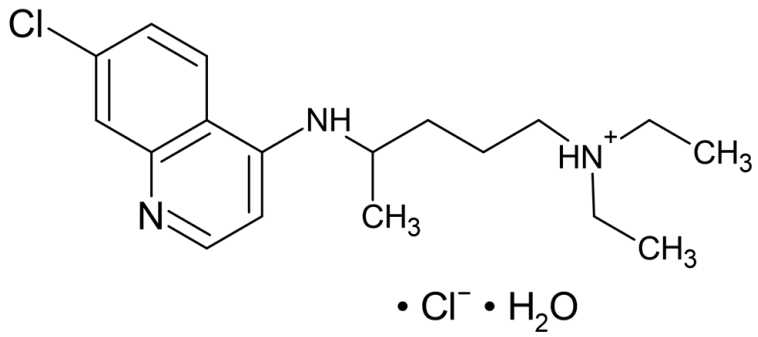

Scheme 1. Structural formula of **CQHCl·H$_2$O**.

2. Results

2.1. Solid-State Structure

Single-crystal X-ray diffraction data show that the **CQHCl·H$_2$O** (N^4-(7-chloroquinolin-4-yl)-N^1,N^1-diethylpentane-1,4-diamine hydrochloride monohydrate) compound crystallizes in the monoclinic space group $P2_1/c$, with one mono-protonated chloroquine cation (CQH^+), one chloride anion (Cl^-), and one water molecule in the asymmetric unit (Figure 1). In the chloroquine cation, as expected, the proton resides on the terminal diethylamino group. The chloroquine molecule adopts a condensed (folded) conformation in which the flexible diamino side chain loops back toward the aromatic core, creating a cavity (224.90 Å^3, 11.2% unit cell volume, and probe 1.2 Å) that accommodates both the water molecule and the chloride anion, thereby maximizing attractive intermolecular interactions. Volumetric analysis indicates that this region forms isolated pockets within the crystal framework, lacking any detectable pathways for water molecule egress.

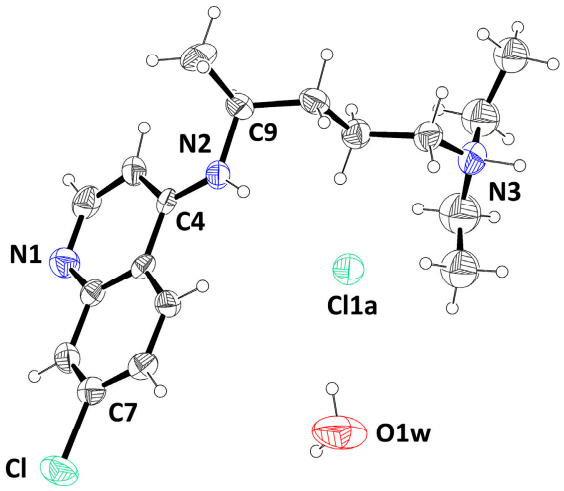

Figure 1. A displacement ellipsoid plot (30% probability) of the asymmetric unit of the centrosymmetric **CQHCl·H$_2$O** crystal structure. Only the isotropically refined atoms of the major disorder component of the pendant diethylamine moiety are shown as spheres. Hydrogen atoms are depicted as small spheres of arbitrary radius. Atoms are coloured according to the following conventional scheme: C, black; N, blue; Cl, green; O, red; and H, white. The standard atom-labelling scheme for the quinoline ring is used.

The quinoline double-ring shows a slight distortion from the planarity with an rms deviation from the best-fit plane of 0.0348 Å and an out-of-plane deformation, measured by the torsion angle ϑ (C2–C3···C6–C7), of −2.81°.

The nitrogen atom of the secondary amine exhibits near-planarity, with a sum of bond angles (∑N) of 359.74°, closely approaching 360°, and an out-of-plane deviation (ΔN) of 0.032 Å, relative to its bonded atoms. The N-C(pyridyl) bond length of 1.331(8) Å is significantly shorter than a typical single bond indicating partial double-bond character arising from imino-type resonance. Additionally, the amino group is twisted out of the plane of the quinoline ring by an angle (φ) of 14.26°.

Comparison of the CQ and **CQHCl·H$_2$O** crystal structures shows large conformational rearrangements upon protonation of the most basic nitrogen atom (4-diethylamino-1-methylbutyl-amino moiety). In Figure 2, the conformations of unprotonated CQ and the doubly protonated dihydrogen phosphates of chloroquine (see caption of Figure 2) are depicted with colour coding of the different crystal structures. Apart from the mono- and dihydrated dihydrogen phosphate salts, which share almost the same conformation (red and light green chains in (Figure 2)) while having significantly different crystal structures, all 4-diethylamino-1-methylbutyl-amino chains adopt different conformations, both in terms of internal C–C–C–C torsional angles and the rotation of the dangling group with respect to the quinoline frame. This happens due to the large number of freely rotating C–C single bonds that are adjusted for minimizing the lattice energy during crystallization, which frequently requires the presence of solvent molecules in the crystal structure. Interestingly, the conformation of the present hydrochloride partly overlaps with the neutral CQ molecule up to the last butyl carbon atom, leaving only the N(ethyl)$_2$ terminal moiety with different orientations (with heavy disorder of the ethyl groups in the monocation).

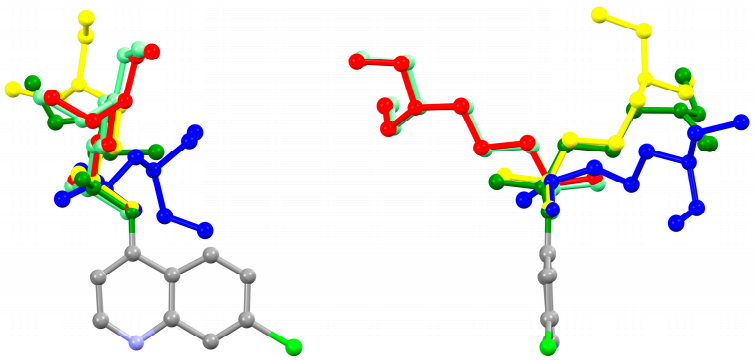

Figure 2. Superposition of chloroquine fragments as observed in the neutral molecule and in various salts in their pertinent crystal structures. Colours of the alkyl chain are yellow neutral CQ (refcode CDMQUI [13]); blue $(CQH_2^{2+})(H_2PO_4)_2$ (refcode HOJLOI [10]); red $(CQH_2^{2+})(H_2PO_4^{-})_2{\cdot}H_2O$ (refcode CLQUON01 [11]); light green $(CQH_2^{2+})(H_2PO_4^{-})_2{\cdot}2H_2O$ (refcode GEXXAI02 [12]); and green $(CQH^{+})(Cl^{-}){\cdot}H_2O$ (present paper). The terminal ethyl groups are ill-defined due to disorder. (**Left**) Front view orthogonal to the quinoline rings. (**Right**) Side view to enhance conformational diversity displacement ellipsoid plot (30% probability level) of the structure of **CQHCl·H$_2$O**. Thermal ellipsoids were drawn at room temperature (RT) and H atoms are shown as small spheres of arbitrary radius. Atoms are depicted using the conventional colour scheme (C: black; N: blue; Cl: green; O: red; and H: white).

2.2. Intermolecular Interaction Analysis

The crystal packing of **CQHCl·H$_2$O** is stabilized by a large number of intermolecular O—H···N, O—H···Cl, and N—H···Cl hydrogen bonds, generating an extensive bidimensional supramolecular arrangement extended along the (1 0 −2) plane (Figure 3).

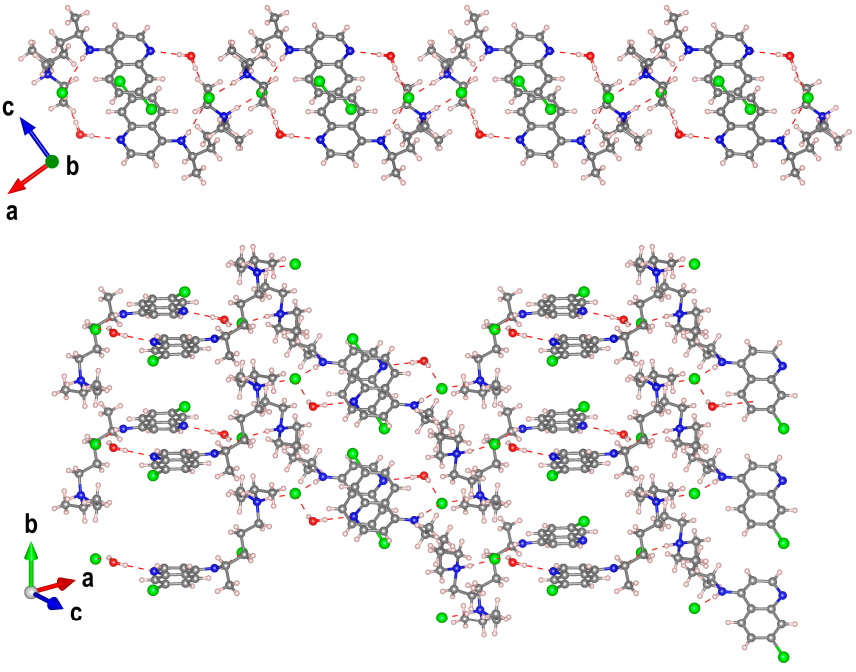

Figure 3. Views along two different directions of the (1 0 −2) bidimensional supramolecular arrangement of the title compound established by classical hydrogen-bonding interactions (red dashed lines). The following two distinct interaction motifs can be readily identified and described using graph-set formalism: R4,6(20) (acceptor: Cl and pyridinic N; donor: H_2O and N-H of the secondary amine) and C1,2(9) (acceptor: Cl; donor: N-H of secondary amine; and N-H of protonated tertiary amine).

The water molecule functions as a double hydrogen-bond donor to the quinoline nitrogen atom and the chloride anion (O···N and Cl distance (Å), O—H···N and Cl angle

(○): 2.875(9), 179(1); 3.258(8), 156(1)) (Table S2), and its oxygen atom serves as a hydrogen-bond acceptor in a weak intermolecular C—H···O contact involving a methyl group of the pendant diethylamine (C—H···O = 3.73(2) Å) (Figure 4).

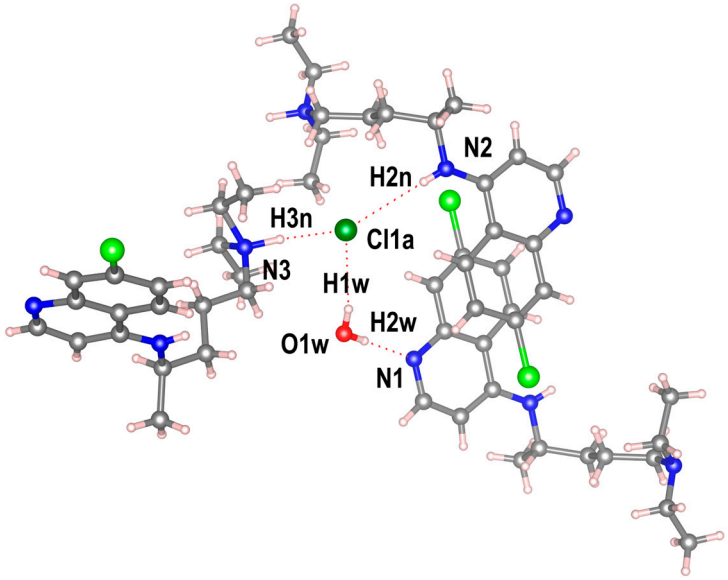

Figure 4. Details of the classic hydrogen bonding (red dashed line) in the title compound.

Similarly, the chloride anion acts as a proton acceptor from the water molecule, the secondary aniline-type nitrogen of a chloroquine molecule, and the protonated tertiary amino nitrogen of a nearby CQH^+ species (Figure 4) (N···Cl distance (Å), N—H···Cl angle (○): 3.522(9), 163(8); 3.098(8), 174(5)) (Table S2). A more detailed analysis further uncovers an array of weak intramolecular C—H···Cl interactions that engage residues from both the side chain and the aryl ring of three adjacent chloroquine molecules. An empirical evaluation of the H-bond strengths in terms of the acid-base parameters has been performed and reported in ESI.

Around the inversion centres at (½, ½, and ½) and (½, 0, and 0), pairs of cations are arranged in a parallel fashion (Figure S1), with a separation of 3.431 Å between their least-squares quinoline planes and a relative orientation angle of 0°. The interring distance and the degree of molecular overlap indicate substantial π–π interactions, further reinforced by face-on contacts involving the aromatic chlorine atom. The "*Aromatics Analyser*" tool in CSD-Materials [14] classifies these aromatic interactions as strong π–π contacts, with a score of seven (see ESI).

The analysis of the Hirshfeld surface (HS) and 2D fingerprints (FPs) performed using *CrystalExplorer* (version 21.5) [15] to study and evaluate intermolecular interactions within the crystal packing of the compound under examination (Figures 5 and S2 and S3) confirmed the above description. The greatest contribution to the HS comes from the H···H contacts (57.8%), due to the large hydrogen content of the molecule, including the presence of very close contacts between the terminal methyl H atoms at a shortest distance of ca. 2.0 Å (the pointed feature a on the diagonal in Figure 5). The FP displays two distinct pairs of sharp spikes corresponding to the hydrogen-bond contacts. The outer and shorter spikes ending at (d_e, d_i) ≅ (1.3, 0.7) Å (and vice versa) correspond to the N–H···Cl hydrogen bonds while the inner longer ones correspond to the O_{water}—H···$N_{pyridinic}$ hydrogen bond, with their tips at $d_e + d_i$ ~1.8 Å.

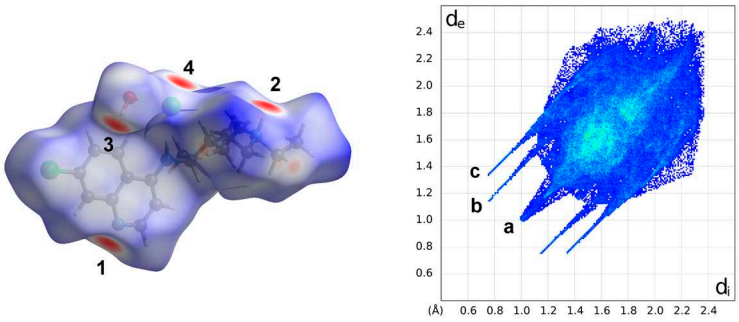

Figure 5. (**Left**) Hirshfeld surface representations for compound **CQHCl·H_2O** with the function d_{norm} plotted onto the surface. Colour code −0.57 Å (red) to 1.61 Å (blue). The red spots are the result of the O_{water}—H···$N_{pyridinic}$ hydrogen bonds (labelled 1 and 3) and $N_{tertiary\ amine}$—H···Cl_{anion} hydrogen bonds (labelled 2 and 4). (**Right**) Overall two-dimensional fingerprint plots for the title compound plot d_e versus d_i. The labels represent interactions between different atoms as follows: (a) H···H, (b) (O—)H···N, and (c) (N—)H···Cl. Given that the plots are symmetrical, the labels can be mirrored through the diagonal.

A careful inspection of the decomposed fingerprint plots, depicted in Figure S3, pointed out that weak π···π interactions within the crystals, equivalent to C···C contacts, represent only 2.5% of surface area and appear as an arrow-shaped distribution at 1.8 Å < (d_i + d_e) < 2.1 Å. Furthermore, the role of the oxygen atom of water as an acceptor in a weak intermolecular hydrogen bond C—H···O, with a pendant methyl group, is highlighted by the hidden pair of large peaks, with d_e + d_i peaks at ≅2.6 Å.

A detailed discussion and rationalization of the close molecular contacts in the crystal structure, based on the electrostatic potential, is provided in the Supplementary Information.

The comparison of these results with the Hirshfeld surface analyses conducted separately on CQH^+, chloride anion, and water molecule reveals that hydrogen bonding dominates both the interactions between the component and the supramolecular assembly together with other short contacts, involving all components.

3. Discussion

For the first time, a chloroquine salt, **CQHCl·H_2O**, containing exclusively monoprotonated chloroquine has been obtained via heterogeneous crystallization and fully characterized crystallographically. X-ray diffraction reveals protonation of CQ at the tertiary aliphatic nitrogen, along with an extensive hydrogen-bond network involving all components of the crystal. Crystallization was achieved by mixing equimolar solutions of neutral CQ in dichloromethane and iron (II) dichloride in methanol. During this process, the chloroquine molecule underwent protonation through proton transfer from the solvent environment, which, in the presence of an appropriate counterion, can favour stabilization of the salt rather than the neutral molecular species.

Spontaneous protonation of the tertiary amine of CQ in methanol in the presence of metal halides has previously been observed in the synthesis of the zwitterionic complexes [M(CQH^+)Cl_3] (M = Zn, Cd), in which the metal cation coordinates to the aromatic N-atom of a chloroquinium ligand [16–18]. The isolation of chloroquine as a simple salt, rather than as a metal complex, is likely governed by the intrinsic reactivity of CQ toward the metal used and by the relative solubilities of the species present in solution. Analogous behaviour has also been observed for piperaquine (PIP), for which both a complex containing a monoprotonated PIP ligand and a halide salt of protonated PIP molecules have been isolated in the presence of metal salts and methanol [19].

Beyond direct protonation, the presence of salts can influence the crystallization environment throughout the entire process, generating alternative solid forms [20]. This phenomenon can be rationalized in terms of ionic strength variations, which modulate the solubility of competing phases and the complex interplay of chemical equilibria, including metal-ligand complexation. A notable example is the selective production of a new dihydrate form of the dihydrochloride salt of amodiaquine (AQ), another well-known antimalarial agent, from a mixture containing magnesium chloride and the previously known form of the AQ salt [21]. Overall, this work highlights the importance of evaluating the effects of excipients on the resulting solid forms and demonstrates that heterogeneous crystallization can serve both as a powerful strategy for the discovery of new crystalline phases and as an effective alternative for systems that are otherwise challenging to crystallize [22]. Comparable approaches have been successfully employed in both pharmaceutical and agrochemical research [23,24]. Nevertheless, further mechanistic investigations into the crystallization processes are required to elucidate how specific metal salts modulate crystallization pathways, thereby promoting the formation of unexpected or distinct solid forms.

4. Materials and Methods

4.1. Materials

The Sigma-Aldrich (Milano, Italy) products—chloroquine diphosphate salt, CQDP, CAS number 50-63-5 ($C_{18}H_{26}ClN_3 \cdot 2H_3PO_4$, 98.5–101.0% EP), iron (II) chloride tetrahydrate ($FeCl_2 \cdot 4H_2O$, ≥99.0%), and sodium hydroxide (NaOH, ACS reagent, ≥97.0%, pellets)—were purchased from Merk Life Science S.r.l., Milano, Italy. All the solvents (dichloromethane, methanol, and n-hexane) were purchased from commercial suppliers (Merk Life Science S.r.l., Milano, Italy) and were ACS or HPLC grade with mass purities higher than 99%. The materials were used as received, without any further purification.

4.2. Synthesis

4.2.1. Free-Base CQ

A well-defined procedure was established to obtain highly crystalline chloroquine (CQ) powder from its salt form. Commercially available racemic chloroquine diphosphate (CQDP, 4.5 to 5 g) was dissolved in 100 mL of water in a 250 mL beaker under stirring. A 1 M sodium hydroxide solution (60 mL) was then added very slowly over approximately one hour with continuous stirring until CQ precipitated as a gel-like substance at the bottom of the beaker. The alkaline supernatant (pH ~9) was removed. The gel was converted into a powder by adding approximately 100 mL of hexane under vigorous manual and magnetic stirring. The suspension was subsequently stirred for at least 3 h. The resulting white solid was recovered by vacuum filtration or by allowing the solvent to evaporate to dryness and then dried in an oven at 40 °C for 12 h. The process yielded the product with an average yield of 80%. To confirm the purity and crystalline nature of the material, all samples were ground and characterized by X-ray powder diffraction (Figure S6).

4.2.2. Salt Crystallization

Single crystals of **CQHCl·H_2O** were obtained by heterogeneous diffusion crystallization. A methanolic solution of $FeCl_2 \cdot 4H_2O$ (8.0 mg, 0.042 mmol in 2.5 mL MeOH) was carefully layered over a dichloromethane solution (2.5 mL) of CQ (23.9 mg, 0.0747 mmol in 2.5 mL CH_2Cl_2) in a glass vial. A small amount of brown precipitate formed immediately. The vial was stoppered and the solutions were allowed to diffuse slowly. After several days, the vial was opened and the mixture was allowed to evaporate at ambient temperature. Slow solvent evaporation to approximately one-third of the initial volume

afforded pale-yellow single crystals suitable for analysis. Partial oxidation of Fe(II) during the crystallization process resulted in the formation of a brown precipitate.

4.3. Single-Crystal X-Ray Diffraction

The single-crystal X-ray data collection for **CQHCl·H_2O** was performed at ambient temperature on an air-stable single crystal mounted on a glass fibre at a random orientation on a Bruker SMART diffractometer (Madison, WI, USA) [25] equipped with an Apex II CCD detector. Graphite-monochromated Mo Kα radiation (λ = 0.71073 Å) at a nominal power of 50 kV × 30 mA was used in conjunction with an ω–scan collection strategy (width of 0.5° $frame^{-1}$; exposure time of 50 secs. per frame) within the limits 1.5°< θ < 20.8°. Cell parameters were retrieved and refined using SAINT software v8.34A [26] on 1393 reflections (16% of the collected reflections). SAINT and SADABS [26] programmes were employed, respectively, to perform data processing and an empirical absorption correction applying a multi-scan method. The structures were solved by direct methods (SIR2019) and refined within the spherical atom approximation by full-matrix least squares on F^2 (SHELX 2018) [27] with the WINGX (2023.1) interface [28]. The structure pictures were generated using the ORTEPIII (v1.0.3) [28] and VESTA (v3.5.8) programmes [29]. The hydrogen-bonding analysis was carried out using the SHELX and PLATON programmes [27,30].

The amino and water H-atoms were located in the difference Fourier map and refined with fixed individual displacement parameters, using a riding model with U_{iso}(H) = 1.2 U_{eq} (O) and U_{iso}(H) = 1.5 U_{eq} (N). All other hydrogen atoms were placed in calculated positions (HFIX 43 for aromatic rings, HFIX 13 for methine group, HFIX 23 for methylene groups, and HFIX 33 for methyl groups) and were included in the refinement in the riding model approximation, with U_{iso} values set to 1.5 U_{eq} (parent atom) for CH_3 and 1.2 U_{eq} (parent atom) for CH and CH_2 groups. All non-H atoms were refined with full occupancies and anisotropic displacement parameters except for those corresponding to disordered entities. The two pendant ethyl groups of the protonated tertiary amine moiety exhibit positional disorder over two sites, with refined occupancy ratios of 54:46% and 72:28%, respectively. All disordered N—CH_2— and CH_3—CH_2— distances were restrained to be equal within errors using the SADI instruction.

Crystal data and refinement details for **CQHCl·H_2O** are as follows: $C_{18}H_{29}Cl_2N_3O$, M_r = 374.34, T = 296(2) K, λ = 0.71073 Å, Monoclinic, space group $P2_1/c$, a = 14.577(4), b = 8.523(2), c = 17.593(5) Å, β = 112.863(3)°, V = 2014.0(9) $Å^3$, Z = 4, ρ_{calc} = 1.235 $g{\cdot}cm^{-3}$, μ_{calc} = 0.332 mm^{-1}, F(000) = 800, θ range = 1.5–20.8°, 8476 reflections collected, 2107 reflections unique, R_{int} = 0.1394, observed reflections [$I > 2\sigma(I)$] 1105, 1 restraints, 227 parameters, R_1 (all data) = 0.1523, wR_2 (all data) = 0.1504, R_1 (observed) = 0.0767, wR_2 (observed) = 0.1303, $\Delta\rho_{max}$ = 0.224 $eÅ^{-3}$, and $\Delta\rho_{min}$ = −0.223 $eÅ^{-3}$.

4.4. X-Ray Powder Diffraction

Ambient X-ray powder diffraction measurements were performed using a Miniflex-600 diffractometer (Rigaku Corporation, Tokio, Japan) with Cu Kα (λ = 1.540598 Å) radiation, at a formal power of 50 kV × 40 mA, over an angular range of 3–40° (2θ), and with an incremental step size of 0.02° (2θ) and a counting time of 1.5 $s{\cdot}step^{-1}$. Phase identification was performed by comparing the experimental powder pattern with that simulated from single-crystal data (CDMQUI from the Cambridge Structural Database) [13]. The analysis of PXRD data was carried out by using Mercury 4.0 software [14].

Supplementary Materials: The following supporting information are available online. Figure S1: π-π interactions in quinoline dimer; Table S1: Aromatic analyser score in **CQHCl·H_2O** (distances and angles of π···π and C–H···π stacking with X as the centre of the aromatics); Table S2: Hydrogen-bond geometry (Å, °) for **CQHCl·H_2O**; Empirical evaluation of the hydrogen bond strength; Figure S2: Relative contributions of various intermolecular interactions to the Hirshfeld surface area in **CQHCl·H_2O**; Figure S3: The decomposed fingerprint plots (atom–atom interactions) of the Hirshfeld surface for **CQHCl·H_2O**; Molecular Electrostatic Potential Analysis; Figure S4: Plots of total electron density isosurfaces mapped with electrostatic potential values; Figure S5: Packing diagram of **CQHCl·H_2O** structure down the [010] direction; Figure S6: The comparison between the experimental data for deprotonated CQ powder and the simulated PXRD pattern from the single-crystal X-ray data of neutral chloroquine. References [31–33] are cited in the Supplementary Materials.

Author Contributions: Conceptualization, methodology, validation, formal analysis, S.R.; investigation, S.R. and M.M.; resources, S.R.; data curation, S.R. and M.M.; writing—original draft, writing—review and editing, S.R. and M.M. All authors have read and agreed to the published version of the manuscript.

Funding: Università degli Studi di Milano is acknowledged for funding this work through the Research Support Plan 2025 (Piano di Sostegno alla Ricerca 2025); grant number PSR2025_DIP_005_SRIZZ.

Data Availability Statement: CCDC 2518893 contains the supplementary crystallographic data for this paper. The data can be obtained free of charge from the Cambridge Crystallographic Data Centre via www.ccdc.cam.ac.uk/structures (accessed on 26 December 2025).

Acknowledgments: Università degli Studi di Milano is acknowledged for funding this research through the program PSR2025.

Conflicts of Interest: The authors declare no conflicts of interest. The funders had no role in the design of the study; the collection, analyses, or interpretation of data; the writing of the manuscript; or the decision to publish the results.

Abbreviations

The following abbreviations are used in this manuscript:

CQ	Chloroquine
CQHCl·H_2O	Chloroquine hydrochloride monohydrate
CQDP	Chloroquine diphosphate
AQ	Amodiaquine
PIP	Piperaquine
HCQ	Hydroxychloroquine
PXRD	X-ray powder diffraction
HS	Hirshfeld surface
FP	Two-dimensional fingerprints plot

References

1. Zhou, W.; Wang, H.; Yang, Y.; Chen, Z.-S.; Zou, C.; Zhang, J. Chloroquine against Malaria, Cancers and Viral Diseases. *Drug Discov. Today* **2020**, *25*, 2012–2022. [CrossRef]
2. Al-Bari, M.A.A. Chloroquine Analogues in Drug Discovery: New Directions of Uses, Mechanisms of Actions and Toxic Manifestations from Malaria to Multifarious Diseases. *J. Antimicrob. Chemother.* **2015**, *70*, 1608–1621. [CrossRef]
3. Shah, S.M.A.; Rasheed, T.; Rizwan, K.; Bilal, M.; Iqbal, H.M.N.; Rasool, N.; Toma, S.; Marceanu, L.G.; Bobescu, E. Risk Management Strategies and Therapeutic Modalities to Tackle COVID-19/SARS-CoV-2. *J. Infect. Public Health* **2021**, *14*, 331–346. [CrossRef]
4. Verbeeck, R.K.; Junginger, H.E.; Midha, K.K.; Shah, V.P.; Barends, D.M. Biowaiver Monographs for Immediate Release Solid Oral Dosage Forms Based on Biopharmaceutics Classification System (BCS) Literature Data: Chloroquine Phosphate, Chloroquine Sulfate, and Chloroquine hydrochloride. *J. Pharm. Sci.* **2005**, *94*, 1389–1395. [CrossRef]
5. Browning, D.J. Pharmacology of Chloroquine and Hydroxychloroquine. In *Hydroxychloroquine and Chloroquine Retinopathy*; Springer: New York, NY, USA, 2014; pp. 35–63. ISBN 978-1-4939-0597-3.

6. De Souza Santos, M.; De Morais Del Lama, M.P.F.; Siuiti Ito, A.; Zumstein Georgetto Naal, R.M. Binding of Chloroquine to Ionic Micelles: Effect of pH and Micellar Surface Charge. *J. Lumin.* **2014**, *147*, 49–58. [CrossRef]
7. Espeau, P. Special Issue "Pharmaceutical Solid Forms: From Crystal Structure to Formulation". *Pharmaceutics* **2025**, *17*, 312. [CrossRef]
8. Iredale, J.; Fieger, H.; Wainer, I.W. Determination of the Stereoisomers of Hydroxychloroquine and Its Major Metabolites in Plasma and Urine Following a Single Oral Administration of Racemic Hydroxychloroquine. *Semin. Arthritis Rheum.* **1993**, *23*, 74–81. [CrossRef] [PubMed]
9. Kalia, S.; Dutz, J.P. New Concepts in Antimalarial Use and Mode of Action in Dermatology. *Dermatol. Ther.* **2007**, *20*, 160–174. [CrossRef] [PubMed]
10. Albesa-Jové, D.; Pan, Z.; Harris, K.D.M.; Uekusa, H. A Solid-State Dehydration Process Associated with a Significant Change in the Topology of Dihydrogen Phosphate Chains, Established from Powder X-Ray Diffraction. *Cryst. Growth Des.* **2008**, *8*, 3641–3645. [CrossRef]
11. Furuseth, S.; Karlsen, J.; Mostad, A.; Romming, C.A.; Salmén, R.; Tønnesen, H.H.; Tokii, T. N4-(7-Chloro-4-Quinolinyl)-N1,N1-Diethyl-1,4-Pentanediamine. An X-Ray Diffraction Study of Chloroquine Diphosphate Hydrate. *Acta Chem. Scand.* **1990**, *44*, 741–745. [CrossRef]
12. Macetti, G.; Loconte, L.; Rizzato, S.; Gatti, C.; Presti, L.L. Intermolecular Recognition of the Antimalarial Drug Chloroquine: A Quantum Theory of Atoms in Molecules-Density Functional Theory Investigation of the Hydrated Dihydrogen Phosphate Salt from the 103 K X-Ray Structure. *Cryst. Growth Des.* **2016**, *16*, 6043–6054. [CrossRef]
13. Courseille, C.; Busetta, B.; Hospital, M. 7-Chloro-4(4-Diethylamino-1-Methylbutyl-Amino) Quinoline. *Cryst. Struct. Commun.* **1973**, *2*, 283.
14. Macrae, C.F.; Sovago, I.; Cottrell, S.J.; Galek, P.T.A.; McCabe, P.; Pidcock, E.; Platings, M.; Shields, G.P.; Stevens, J.S.; Towler, M.; et al. *Mercury 4.0*: From Visualization to Analysis, Design and Prediction. *J. Appl. Crystallogr.* **2020**, *53*, 226–235. [CrossRef] [PubMed]
15. Spackman, P.R.; Turner, M.J.; McKinnon, J.J.; Wolff, S.K.; Grimwood, D.J.; Jayatilaka, D.; Spackman, M.A. CrystalExplorer: A Program for Hirshfeld Surface Analysis, Visualization and Quantitative Analysis of Molecular Crystals. *J. Appl. Crystallogr.* **2021**, *54*, 1006–1011. [CrossRef] [PubMed]
16. Soave, R. *CCDC 2130150: Experimental Crystal Structure Determination*; Cambridge Crystallographic Data Centre: Cambridge, UK, 2021.
17. Paulikat, M.; Vitone, D.; Schackert, F.K.; Schuth, N.; Barbanente, A.; Piccini, G.; Ippoliti, E.; Rossetti, G.; Clark, A.H.; Nachtegaal, M.; et al. Molecular Dynamics and Structural Studies of Zinc Chloroquine Complexes. *J. Chem. Inf. Model.* **2023**, *63*, 161–172. [CrossRef]
18. Squarcina, A.; Franke, A.; Senft, L.; Onderka, C.; Langer, J.; Vignane, T.; Filipovic, M.R.; Grill, P.; Michalke, B.; Ivanović-Burmazović, I. Zinc Complexes of Chloroquine and Hydroxychloroquine versus the Mixtures of Their Components: Structures, Solution Equilibria/Speciation and Cellular Zinc Uptake. *J. Inorg. Biochem.* **2024**, *252*, 112478. [CrossRef]
19. Rizzato, S. Dipartimento di Chimica, Università Degli Studi di Milano, Milano, Italy. 2026; *Unpublished results (Manuscript in Preparation)*.
20. Cotting, G.; Urquidi, O.; Besnard, C.; Brazard, J.; Adachi, T.B.M. The Effect of Salt Additives on the Glycine Crystallization Pathway Revealed by Studying One Crystal Nucleation at a Time. *Proc. Natl. Acad. Sci. USA* **2025**, *122*, e2419638122. [CrossRef]
21. Putra, O.D.; Pettersen, A.; Nilsson Lill, S.O.; Umeda, D.; Yonemochi, E.; Nugraha, Y.P.; Uekusa, H. Capturing a New Hydrate Polymorph of Amodiaquine Dihydrochloride Dihydrate *via* Heterogeneous Crystallisation. *CrystEngComm* **2019**, *21*, 2053–2057. [CrossRef]
22. Takenaka, H.; Kawashima, Y.; Lin, S.Y. Polymorphism of Spray-Dried Microencapsulated Sulfamethoxazole with Cellulose Acetate Phthalate and Colloidal Silica, Montmorillonite, or Talc. *J. Pharm. Sci.* **1981**, *70*, 1256–1260. [CrossRef]
23. Tipduangta, P.; Takieddin, K.; Fábián, L.; Belton, P.; Qi, S. A New Low Melting-Point Polymorph of Fenofibrate Prepared via Talc Induced Heterogeneous Nucleation. *Cryst. Growth Des.* **2015**, *15*, 5011–5020. [CrossRef]
24. Braga, D.; Grepioni, F.; Chelazzi, L.; Nanna, S.; Rubini, K.; Curzi, M.; Giaffreda, S.L.; Saxell, H.E.; Bratz, M.; Chiodo, T. Bentazon: Effect of Additives on the Crystallization of Pure and Mixed Polymorphic Forms of a Commercial Herbicide. *Cryst. Growth Des.* **2014**, *14*, 5729–5736. [CrossRef]
25. Bruker. *APEX2 V2014.1-1*; Bruker AXS Inc.: Madison, WI, USA, 2015.
26. Bruker. *SAINT v8.34A; XPREP V2013/3, SADABS*; Bruker AXS Inc.: Madison, WI, USA, 2013.
27. Sheldrick, G.M. Crystal Structure Refinement with SHELXL. *Acta Crystallogr. Sect. C Struct. Chem.* **2015**, *71*, 3–8. [CrossRef] [PubMed]
28. Farrugia, L.J. WinGX and ORTEP for Windows: An Update. *J. Appl. Crystallogr.* **2012**, *45*, 849–854. [CrossRef]
29. Momma, K.; Izumi, F. VESTA 3 for Three-Dimensional Visualization of Crystal, Volumetric and Morphology Data. *J. Appl. Crystallogr.* **2011**, *44*, 1272–1276. [CrossRef]

30. Spek, A.L. Single-Crystal Structure Validation with the Program *PLATON*. *J. Appl. Crystallogr.* **2003**, *36*, 7–13. [CrossRef]
31. Gilli, P.; Pretto, L.; Bertolasi, V.; Gilli, G. Predicting Hydrogen-Bond Strengths from Acid−Base Molecular Properties. The pK_a Slide Rule: Toward the Solution of a Long-Lasting Problem. *Acc. Chem. Res.* **2009**, *42*, 33–44. [CrossRef]
32. Lippincott, E.R.; Schroeder, R. One-Dimensional Model of the Hydrogen Bond. *J. Chem. Phys.* **1955**, *23*, 1099–1106. [CrossRef]
33. Ryckaert, J.-P.; Ciccotti, G.; Berendsen, H.J.C. Numerical Integration of the Cartesian Equations of Motion of a System with Constraints: Molecular Dynamics of n-Alkanes. *J. Comput. Phys.* **1977**, *23*, 327–341. [CrossRef]